BIOLOGY OF REPRODUCTION (2015) **93**(6):137, 1–12
Published online before print 21 October 2015.
DOI 10.1095/biolreprod.115.134940

Disrupting Cyclin Dependent Kinase 1 in Spermatocytes Causes Late Meiotic Arrest and Infertility in Mice[1]

Tracy M. Clement,[4] Amy L. Inselman,[3,4] Eugenia H. Goulding, William D. Willis, and Edward M. Eddy[2]

Gamete Biology Group, Reproductive and Developmental Biology Laboratory, National Institute of Environmental Health Sciences, National Institutes of Health, Research Triangle Park, North Carolina

ABSTRACT

While cyclin dependent kinase 1 (CDK1) has a critical role in controlling resumption of meiosis in oocytes, its role has not been investigated directly in spermatocytes. Unique aspects of male meiosis led us to hypothesize that its role is different in male meiosis than in female meiosis. We generated a conditional knockout (cKO) of the *Cdk1* gene in mouse spermatocytes to test this hypothesis. We found that CDK1-null spermatocytes undergo synapsis, chiasmata formation, and desynapsis as is seen in oocytes. Additionally, CDK1-null spermatocytes relocalize SYCP3 to centromeric foci, express H3pSer10, and initiate chromosome condensation. However, CDK1-null spermatocytes fail to form condensed bivalent chromosomes in prophase of meiosis I and instead are arrested at prometaphase. Thus, CDK1 has an essential role in male meiosis that is consistent with what is known about the role of CDK1 in female meiosis, where it is required for formation of condensed bivalent metaphase chromosomes and progression to the first meiotic division. We found that cKO spermatocytes formed fully condensed bivalent chromosomes in the presence of okadaic acid, suggesting that cKO chromosomes are competent to condense, although they do not do so in vivo. Additionally, arrested cKO spermatocytes exhibited irregular cell shape, irregular large nuclei, and large distinctive nucleoli. These cells persist in the seminiferous epithelium through the next seminiferous epithelial cycle with a lack of stage XII checkpoint-associated cell death. This indicates that CDK1 is required upstream of a checkpoint-associated cell death as well as meiotic metaphase progression in mouse spermatocytes.

CDK1, cell cycle, chromosome condensation, male meiosis, meiotic arrest, metaphase-promoting factor, okadaic acid, synaptonemal complex

INTRODUCTION

The serine/threonine kinase CDK1 (previously CDC2) dimerizes with cyclin B1 (CCNB1) to form the metaphase-promoting factor (MPF). This activates CDK1 and leads to phosphorylation of proteins involved in cell cycle progression, including microtubule dynamics, nuclear envelope breakdown, nucleolar organization, and chromatin condensation in mitotic cells and in female meiotic germ cells [1–3]. However, previous studies have suggested that the function of CDK1 in male meiosis is not equivalent to that in female germ cells and that other CDKs have essential and unique roles in male meiosis. For example, CDK2 is not required for resumption of meiosis in oocytes [1] but is essential for completion of meiosis in spermatocytes [4, 5]. Also, whereas reentry of oocytes into meiosis I (MI) requires activation of CDK1 by cell division cycle 25B (CDC25B), male CDC25B-null mice are fertile [6–8].

Differences also have been seen in the characteristics of CDK-binding partners in oocytes and spermatocytes. Cyclin A2 (CCNA2) is required for entry into meiosis and sister chromatid separation in oocytes [9] but is not detected in prophase spermatocytes [10]. In addition, deletion of cyclin A1 (CCNA1) results in failure to activate CDK1 kinase activity in spermatocytes and male infertility, but CCNA1-null females are fertile [11, 12]. It also appears that CDK2 acts, at least in part, independently of CCNA1 in spermatocytes. CDK2-null spermatocytes arrest in the pachytene stage, but CCNA1-null spermatocytes arrest later after desynapsis [12, 13]. A testis-specific member of the heat shock protein 70 family, HSPA2, is required for completion of meiosis in spermatocytes but not in oocytes [14]. HSPA2 is a chaperone for CDK1 in spermatocytes. HSPA2-null male mice fail to form MPF, CDK1 kinase activity is not detected, chromosomal desynapsis defects occur, spermatocytes fail to enter metaphase I, and late pachytene- to diplotene-stage spermatocytes undergo apoptosis [14, 15]. Meiotic divisions occur occasionally, possibly due to activities of other kinases [16]. Mutation of the *Eif4g3* gene produces meiotic defects that mimic the HSPA2-null phenotype, and EIF4G3 is required for *Hspa2* translation [17]. Taken together, these findings strongly suggest that unique processes are involved in regulating cell cycle progression in male meiosis, and there are significant differences in how CDKs and their binding partners participate in these events in oocytes and spermatocytes.

Mouse oocytes arrest after the diplotene stage of prophase I in the fetus and luteinizing hormone triggers resumption of meiosis beginning in puberty [18]. A conditional knockout (cKO) of the *Cdk1* gene shows that oocytes lacking CDK1 are able to develop to prophase, but arrest at the germinal vesicle stage and are unable to undergo germinal vesicle breakdown or resume meiosis [1]. We generated a cKO of the *Cdk1* gene in mouse spermatocytes to test the hypothesis that the role of CDK1 in meiosis is different in male germ cells than in female germ cells. The *Cdk1* gene was disrupted at the beginning of prophase I in spermatocytes using *Hspa2*-cre, first expressed in preleptotene spermatocytes [19]. The effect of the cKO on the progression of spermatocytes through meiosis was analyzed using confocal microscopy to examine surface spread chromatin immunolabeled with a panel of previously characterized antibody markers of meiotic processes, including repair of

[1]This work was supported by the Intramural Research Program of the NIH, National Institute of Environmental Health Sciences.
[2]Correspondence: E-mail: eddy@niehs.nih.gov
[3]Current address: Division of Systems Biology, Biomarkers and Alternative Models Branch, National Center for Toxicology Research/ Food and Drug Administration, Jefferson, AR 72079.
[4]These authors contributed equally to this work.

Received: 27 August 2015.
First decision: 18 September 2015.
Accepted: 15 October 2015.

eISSN: 1529-7268 http://www.biolreprod.org
ISSN: 0006-3363

double-strand DNA breaks, centromere and telomere dynamics, frequency of chiasmata, and synaptonemal complex (SC) dynamics. This study provides the first detailed characterization of the role of CDK1 in male meiosis.

MATERIALS AND METHODS

Generation of Mice with a Conditional Deletion (cKO) in the Cdk1 Gene

Animal maintenance and experimental protocols were approved by the Institutional Animal Care and Use Committees of the National Institute of Environmental Health Sciences. To produce the *Cdk1* cKO mice, a targeting vector (Supplemental Fig. S1A; Supplemental Data are available online at www.biolreprod.org) was assembled on a pBluescript II KS (+) backbone (Stratagene). Generation of the targeting vector, transfection and screening of embryonic stem (ES) cells, and production of mice carrying the targeted mutation are described in Supplemental Materials and Methods.

Spermatocyte-specific deletion of *Cdk1* was achieved by crossing $Cdk1^{flox/flox}$ mice to Tg (*Hspa2*-cre)1Eddy mice expressing Cre-recombinase under direction of the *Hspa2* promoter [19]. $Cdk1^{+/flox}$:$Hspa2^{cre+}$ offspring were then mated to $Cdk1^{flox/flox}$ mice to generate wild-type (WT, $Cdk1^{+/flox}$), heterozygous (HET, $Cdk1^{+/flox}$:$Hspa2^{cre+}$ or $Cdk1^{flox/-}$), and cKO ($Cdk1^{flox/-}$:$Hspa2^{cre+}$) mice in which *Cdk1* exon 3 is deleted specifically from postmitotic germ cells at the initiation of meiosis. The *Hspa2*-cre mice were generated for these studies after repeated attempts to use Tg (*Sycp1*-cre)4Min (*Sycp1*-cre) mice to produce CDK1-null spermatocytes were unsuccessful.

Fertility Study

A total of eight *Cdk1* cKO males and eight HET males between 8 and 12 wk old were each mated with two WT 129S6 females for 2 mo. If after the first month no pregnancies occurred, two new females were paired with the male. All the females were monitored for pregnancy for 3–4 wk after separation from the males. Litter dates, number of pups, sex ratios, and genotypes (Mendelian ratios) were recorded for all the resulting litters.

Tissue Collection and Histological Analysis

All adult tissues collected were from males between 3 and 7 mo old. Weights were recorded for whole body, testes, epididymides, seminal vesicles, and spleen. For sperm counts, cauda epididymides were trimmed to remove fat and other tissue and placed into 1 ml of Ca^{++}/Mg^{++}-free phosphate-buffered saline (PBS). Four or five small cuts were made in the epididymides to allow the sperm to swim out. After 15 min at room temperature, the media containing the sperm was collected and counts were obtained using a hemocytometer. The tissue weights and sperm count data were collected for nine WT, 22 HET, and eight cKO males. Testes were collected and processed for analysis of spermatocytes as outlined below, or testes and epididymides were fixed in Bouin solution overnight. Bouin-fixed tissues were dehydrated and embedded in paraffin and sectioned using standard techniques. Tissue sections were cut at 5 μm. Periodic acid Schiff (PAS) staining of polysaccharides was used to identify Golgi complexes in spermatocytes and developing acrosomes in spermatids [20]. Hematoxylin counterstaining with PAS or hematoxylin and eosin staining were performed using standard methods.

Immunoblot Analysis

Proteins were extracted by homogenization of testes in ice-cold cell lysis buffer (50 mM Tris, pH7.5, 150 mM NaCl, 0.1% IGEPAL CA-640 [Fluka], 50 mM NaF, 1 mM Na_3VO_3, 1 mM dithiothreitol) containing 1 mM phenylmethanesulfonyl fluoride and complete miniprotease inhibitor cocktail tablet without ethylenediaminetetraacetic acid (Roche). All the chemicals were from Sigma except where otherwise noted. A dounce homogenizer was used for homogenization before and after 30 min incubation on ice. Extracts were centrifuged 10 min at $14\,000 \times g$ to separate soluble and insoluble fractions. Protein concentrations were determined using a Bradford protein assay (BioRad) according to the manufacturer's instructions. Ten micrograms of the soluble fraction was boiled in SDS buffer for 10 min, separated on a 12% Tris-glycine gel (BioRad), and immunoblotted using standard procedures. Antibodies to CDK1 (SC-54; Santa Cruz), CCNB1 (4135; Cell Signaling), and CCNA1 (SC-15383; Santa Cruz) were used at 1:200, 1:2000, and 1:500 dilutions, respectively. Immunoblots for each antibody were performed with lysates from at least three separate males. Horseradish peroxidase-conjugated goat-anti-mouse or goat-anti-rabbit (Sigma) secondary antibodies were used at 1:20 000 dilutions. Detection was performed using the ECL Plus Detection System (Amersham).

Immunohistochemistry

Bouin-fixed testis sections with paraffin removed were microwaved in antigen retrieval solution (2.9 mM citric acid, 12.3 mM sodium citrate) for 8 min. Sections were incubated in 3% H_2O_2 for 15 min to block endogenous peroxidase and in 10% goat serum (Vector Labs) to block nonspecific antibody binding. Primary antibodies were diluted in 3% goat serum as follows: CDK1 (ab18, 1:100 dilution; Abcam), histone 3, phosphor-serine 10 (H3pS10) (9706, 1:200 dilution; Cell Signaling), heat shock protein A, like 1 (HSPA1L) (1:100 dilution) [21], and glyceraldehyde 3-phosphate dehydrogenase, sperm (GAPDHS) (1:200 dilution) [22]. Vectastain ABC kits and imPACT DAB (Vector Labs) were used for detection according to manufacturer's recommendations. Sections were counterstained with hematoxylin.

In Situ Hybridization

A 271-bp probe spanning *Cdk1* exons three and four was amplified from liver cDNA (*Cdk1* in situ hybridization [ISH] forward: ACGGTGTGGTGTA TAAGGGTAGAC, *Cdk1* ISH reverse: ACGAGTGAAGAATCCAT GAACTGC) and cloned into pGEM-T Easy (Promega) using standard procedures; the construct was sequence verified. The *Cdk1* probe sequence and vector encoded SP6 and T7 polymerase promoters were amplified from the vector (pCU/M13 forward: CGCCAGGGTTTTCCCAGTCACGAC, pCU/M13 reverse: TCACACAGGAAACAGCTATGAC) and gel purified (QIAquick Gel Extraction Kit; Qiagen). A digoxigenin-UTP RNA labeling kit (SP6/T7; Roche) was then used to amplify and label sense and antisense probes using the SP6 and T7 sites, respectively. Hybridization was performed as previously described [23]. Sense probe negative controls were included with each experiment. Sections were counterstained with eosin.

Cell Death Assay

Bouin-fixed testis sections with paraffin removed were incubated in 3% H_2O_2, blocked with 1% horse serum (26050-088; Gibco) and 3% bovine serum albumin (fraction V, 802239; Schwarz/Mann) with 0.5% Triton X-100, and immunolabeled. The sections were incubated with primary SYCP3 antibodies (ab97672 or ab15093; Abcam) diluted 1:200 in blocking buffer followed by anti-mouse or -rabbit Alexa Fluor 546 (Invitrogen) and then by mouse antibody to phosphorylated histone H2A family, member X (H2AFXγ) conjugated to Alexa Fluor 647 (560447, 1:10 dilution; BD Pharmingen). Terminal deoxynucleotidyl transferase dUTP nick-end-labeling (TUNEL) was performed on sections using the In Situ Cell Death Kit with fluorescein-dUTP (Roche) according to the manufacturer's protocol without peroxidase conversion and mounted in Prolong Gold Antifade reagent with 4′,6-diamidino-2-phenylindole (DAPI) (Sigma). Images were acquired using a Zeiss 710 inverted confocal multiphoton laser-scanning microscope with 405, 488, and 561 nm lasers and a Zeiss Plan-Apochromat 63X (1.4 na) oil immersion objective lens. Images were scanned and analyzed using Zenn 2010 software.

Surface Spreads

Spermatocyte surface spread preparation procedures were adapted from previously reported protocols [24, 25]. For 3- to 7-mo-old adults and 18-day-old pubertal animals with spermatocytes in the first wave of spermatogenesis, the tunica albuginea was stripped from testes and the tubules placed into hypotonic extraction buffer (30 mM Tris, pH 8.2, 50 mM sucrose, 17 mM sodium citrate, 5 mM ethylenediaminetetraacetic acid, 2.5 mM dithiothreitol, and 0.5 mM phenylmethanesulfonyl fluoride) at room temperature for 45–60 min. Sections of tubules were placed into a drop of 100 mM sucrose and chopped with fine gauge needles to release germ cells. Superfrost glass slides (Fisher) were coated with a film of 1% paraformaldehyde with 0.2% Triton X-100. A 10 μl suspension of germ cells was added to the wet slide and rocked back and forth to spread the cells over the surface. Slides were placed in a humid chamber at 37°C and allowed to begin drying overnight. The next-day slides were allowed to dry completely and then washed with 0.4% Photoflow (Kodak) for 2 min and dried again.

Surface spreads were immunolabeled using SYCP3 (ab97672 or ab15093, 1:100 dilution; Abcam), SYCP1 (15090, 1:100 dilution; Abcam), telomeric repeat binding factor 1 (TERF1) (TRF12-S, 1:50 dilution; Alpha Diagnostics), anticentromeric antibody (ACA) (15-235, 1:50 dilution; Antibodies Inc.), histone H3, trimethyl K9 (H3K9me3) (ab8898, 1:500 dilution; Abcam), BRCA1 (sc1553, 1:50 dilution; Santa Cruz), ataxia telangiectasia and Rad3

related (ATR) (sc1887, 1:50 dilution; Santa Cruz), H2AFXγ (05-636, 1:1000 dilution; Millipore), and yeast MutL homologue 1 (MLH1) (PC56, 1:75 dilution; Calbiochem). Secondary antibodies produced in donkey (Invitrogen) included: anti-mouse Alexa Fluor 488, anti-mouse Alexa Fluor 546, anti-rabbit Alexa Fluor 488, anti-rabbit Alexa Fluor 546, and anti-goat Alexa Flour 488. A goat anti-human Texas Red secondary (ab6856; Abcam) was used for ACA detection.

Images were obtained using a Zeiss 710 microscope and scanned and analyzed using Zenn 2010 software. Specific stages of prophase I were identified on the basis of the morphology of the SC [26–28] for cells from at least three animals of each genotype. The total number of autosomal MLH1 foci per cell and the occurrence of SYCP3-positive chromosomal fragments at pachynema were determined for at least 30 pachytene-stage spermatocytes from each animal. The numbers of SYCP3 foci in prometaphase were determined for at least 10 spermatocytes from each biological replicate.

Air-Dried Chromosome Preparation and Condensation Assays

A mixed germ cell population was isolated from testes as described previously [29]. Cells were processed by the modified Evans protocol for air-dried chromosomes [30] and Giemsa stained (Gibco) according to manufacturer's recommendations. For induced chromosome condensation, mixed germ cells were cultured in medium with or without okadaic acid (OA) for 5 h before preparation for chromosomal condensation analysis as described previously [31].

Transmission Electron Microscopy

Testes were fixed for transmission electron microscopy (TEM) overnight at 4°C in 0.2% picric acid, 2.5% glutaraldehyde, and 2% paraformaldehyde in 0.1 M sodium phosphate buffer, pH 7.4. Samples were then processed as described previously [32] and examined with a Zeiss 910 TEM with a digital interface and Gatan SC1000 camera located in the Microscopy Services Laboratory, University of North Carolina School of Medicine. Sections from an adult cKO testis were observed by electron microscopy and compared with control (data not shown).

Statistics

GraphPad Prism 6 (version 6.05; GraphPad Software Inc.) and SAS 9.3 (version 9.3; SAS Institute) were used to generate graphs and perform statistical analyses. A one-way ANOVA with Tukey multiple testing correction was used for analysis of tissue and body weights and sperm counts. The fertility study, pachytene-stage SYCP3 fragments, and MLH1 foci analyses were each assessed with two-tailed unpaired *t*-tests. A nested multivariate analysis of variance was used to compare genotypes for the bright and dim prometaphase SYCP3 foci counts where animal was nested within genotype. All the compared values with statistically significant differences had $P < 0.001$, except for pachytene-stage SYCP3 fragments where $P = 0.0248$, and prometaphase SYCP3 foci counts for total foci where $P = 0.0335$. The equality of variance of prometaphase SYCP3 foci counts between genotypes was assessed with a Bartlett F-test for bright, dim, and total foci. For the cell death assays, a two-way ANOVA revealed significant interactions between genotypes for the number of tubules with TUNEL-positive cells. Therefore an additional two-way ANOVA with Tukey multiple testing corrections was used to test for significant differences between genotypes at each stage. For the TUNEL-positive cells per tubule analysis, an initial ANOVA revealed significant interactions between stage and genotype. Therefore, two additional two-way ANOVAs with Tukey multiple testing corrections were performed to test genotype differences per stage and stage differences per genotype. All the experiments, including those without statistical representation, were performed with at least three biological replicates except for the electron microscopy for which observations were from one cKO male.

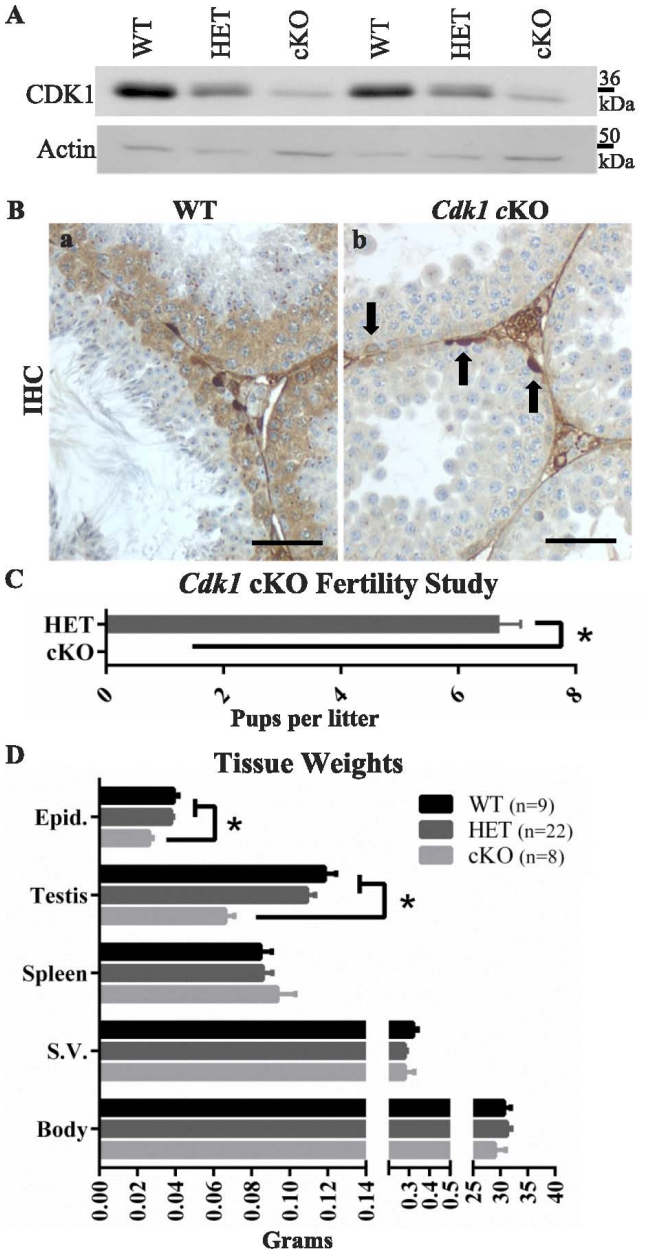

FIG. 1. Targeted deletion of *Cdk1* in mouse spermatocytes. **A**) CDK1 levels in whole testis lysates of *Cdk1* cKO mice are reduced compared to WT or HET testis lysates. **B**) The deletion specifically from meiotic, but not mitotic, male germ cells was confirmed by IHC and ISH. In WT seminiferous tubules, CDK1 localizes to mitotic and meiotic germ cells in the basal half of the seminiferous epithelium (**Ba**, brown labeling). In the cKO seminiferous epithelium, however, only mitotically dividing cells exhibit CDK1 localization (**Bb**, arrows). Bars = 50 μm. **C**) The fertility of HET mice is indicated by the average number of pups per litter compared to the cKO, which was infertile. **D**) Body and organ weights for WT, HET, and cKO males are represented in bar graph form. Error bars indicate SEM; asterisk (*) indicates statistically significant difference.

RESULTS

CDK1 Is Not Present in Spermatocytes of cKO Mice

CDK1 levels in WT, HET, and cKO testes were determined by assaying lysates from adult males by immunoblotting. CDK1 was present in testes of HET and cKO mice, but the levels were reduced in HET and further reduced in cKO mice compared to WT mice (Fig. 1A). The presence of CDK1 in cKO testis lysates was seen by immunohistochemistry (IHC) to be from CDK1 expression in spermatogonia undergoing mitosis (Fig. 1B). The expression of *Cdk1* was confirmed to be restricted to spermatogonia in cKO mice by ISH (Supplemental Fig. S1B). The CCNB1 (Supplemental Fig. S1C) and CCNA1 (Supplemental Fig. S1D) levels did not appear to be different on immunoblots of extracts of testes from cKO, HET, and WT males.

CDK1 Is Required for Male Fertility

The cKO and HET males were mated with WT females to determine the effect of the mutation on fertility. Whereas eight HET males were fertile, producing 37 litters with an average litter size of 6.7 pups, eight cKO males produced no pups, exhibiting infertility (Fig. 1C). No significant differences in body, spleen, or seminal vesicle weights were found between WT, HET, and cKO males. However, cKO mice showed a significant reduction in epididymis and testis weights compared to WT or HET males (Fig. 1D).

Initial studies suggested that testes from cKO mice lacked postmeiotic germ cells (Fig. 1Bb). To examine this more closely, PAS staining (Fig. 2, A–J) was used to determine if acrosome-containing spermatids were present in cKO testes [20]. The PAS stain also recognizes Golgi bodies, and these were seen in late prophase spermatocytes in testes from WT mice (Fig. 2C) and in spermatocytes in cKO mice (Fig. 2D). While PAS-positive acrosomes were seen in testes from WT mice (Fig. 2, E, step 4 spermatid, and G, step 6 spermatid, arrowheads), they were not seen in cKO mice. In the cKO mice, PAS staining was only seen in prophase Golgi (Fig. 2, D and F) and in the cytoplasm of abnormal-appearing cells (Fig. 2F), including multinucleated giant cells (Fig. 2H), which likely resulted from syncytial bridge collapse [33, 34].

In addition, the spermatid-specific HSPA1L and GAPDHS proteins were detected by IHC in testes from WT mice but not in cKO mice (Supplemental Fig. S2). Furthermore, sperm were abundant in the cauda epididymis of WT mice (Fig. 2, I and K) but were not present in cauda epididymis of cKO mice where only large rounded cells and some cellular debris were seen (Fig. 2, J and K). These results indicate that spermatogenesis in cKO mice failed to advance to the postmeiotic phase and that the reduced testis and epididymis weights were due to the lack of spermatids in the testis and of sperm in the epididymis.

Meiosis Progresses to Prometaphase I in cKO Mice

Mouse oocytes arrest after completion of the diplotene stage of meiotic prophase I at the germinal vesicle stage until oocyte maturation and meiotic resumption. CDK1-null oocytes are unable to resume meiotic progression and remain permanently arrested in the germinal vesicle stage [1]. To determine when CDK1 is required for progression through the substages of prophase I in male meiosis, surface spreads of spermatocytes from cKO mice were immunolabeled with antibodies to SC components. The SC is a hallmark feature of meiosis and is involved in the pairing, synapsis, and separation of homologous chromosomes during prophase of the first meiotic division. Antibodies have been used on surface spreads of spermatocytes to localize SC-associated marker proteins on chromosomes as a means of defining progression through the substages of meiotic prophase I [35, 36]. The SC proteins 3 and 1 (SYCP3, SYCP1) are key structural components. SYCP3 is present in the axial elements that form along each chromosome in leptotene and becomes part of the lateral elements when the homologous chromosomes begin to pair during the zygotene stage to initiate synapsis. SYCP1 localizes to the central element of the SC as synapsis proceeds and in the pachytene stage; SYCP3 and SYCP1 are present along the length of each pair of synapsed autosomes. Antibodies to SYCP3 and SYCP1 were used in previous studies to monitor formation of the lateral and central elements of the SC, synapsis of the homologs, removal of the central elements in the diplotene stage, and relocalization of lateral elements to a restricted region at the kinetochores in the diakinesis stage [27, 28, 37–41].

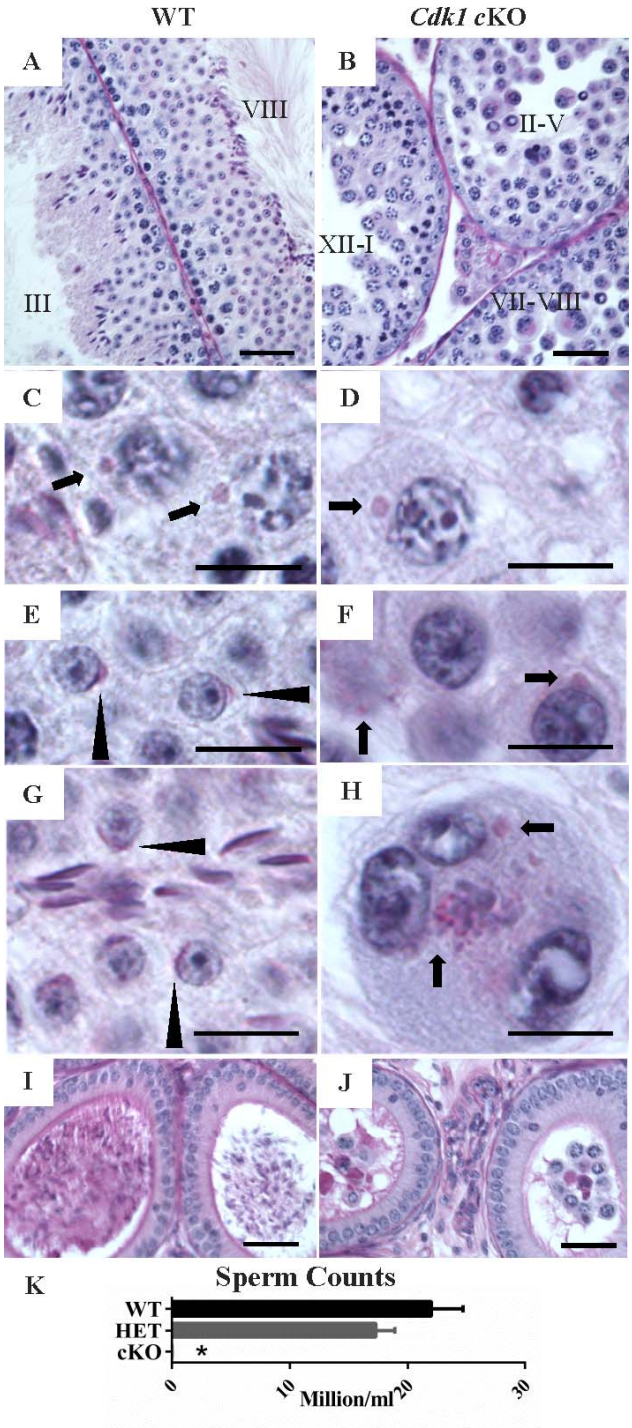

FIG. 2. *Cdk1* cKO testes lacks postmeiotic germ cells. Periodic acid Schiff-hematoxylin (PAS-H)-stained tissue sections. **A**) WT testis sections with stages III and VIII tubules shown. **B**) The cKO testis section with three tubules shown, and approximate tubule stages indicated (II–V, XII–I, and VII–VIII). WT spermatocytes (**C**) and cKO spermatocytes (**D**) (arrow = PAS-positive Golgi). WT spermatids in stage 4 (**E**) and stage 6 (**G**) (arrowhead = steps 4 and 6 spermatids, respectively). **F** and **H**) Abnormal cKO cells from luminal portion of tubules. PAS staining is indicated in the cytoplasm (arrows) of cells in a tubule stage between II and V (**F**) and multinucleated giant cells (**H**). **I**) WT caput epididymal section containing sperm. **J**) The cKO caput epididymal section containing rounded cells and debris but lacking sperm. Bars = 40 μm in **A**, **B**, **I**, and **J**, and 10 μm in **C**–**H**. **K**) Sperm counts in WT, HET, and cKO mice. Error bars indicate SEM; asterisk (*) indicates statistically significant difference.

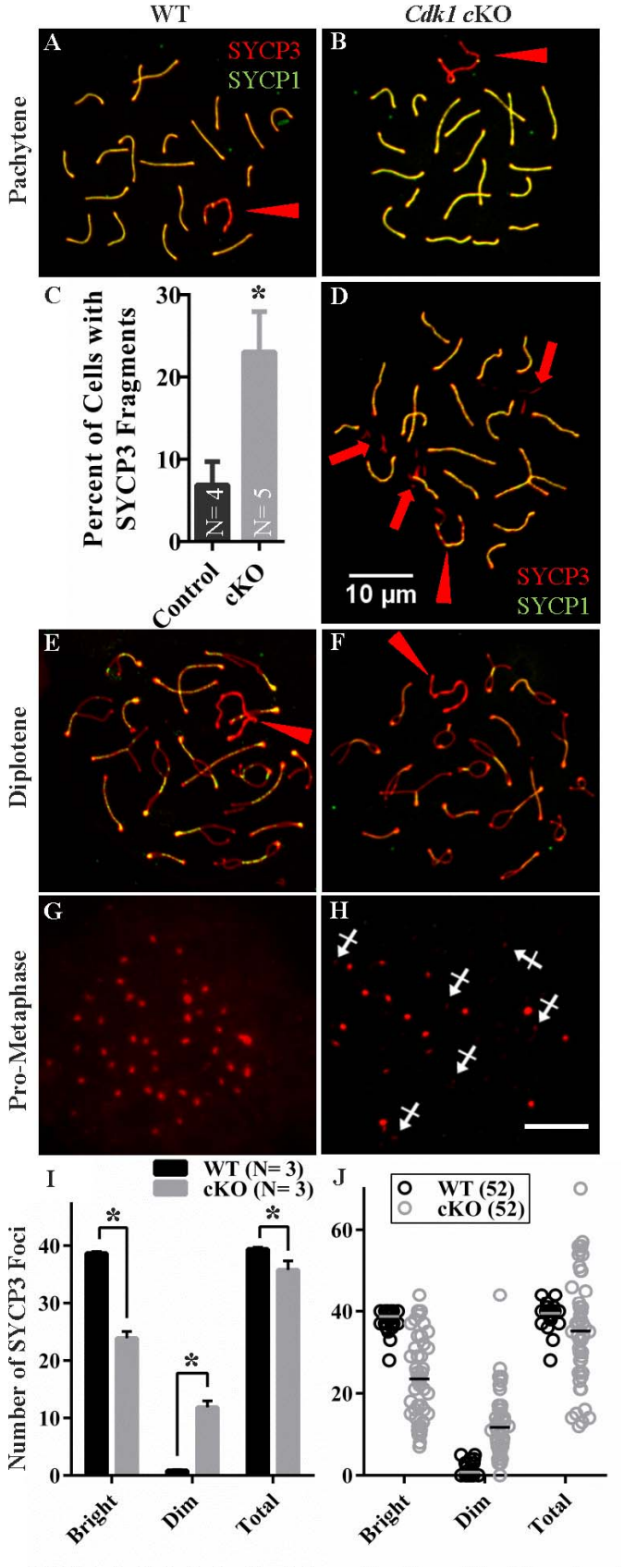

FIG. 3. Normal prophase I progression through diplonema in *Cdk1* cKO testis with extrachromosomal SYCP3 aggregation at pachynema. SYCP3 (red) and SYCP1 (green) labeling of WT (**A**, **E**, **G**) and cKO (**B**, **D**, **F**, **H**) spermatocyte spreads. Fully synapsed chromosomes (colocalized SYCP3 and SYCP1 appear yellow) in WT (**A**) and cKO (**B**) indicative of pachynema. SYCP3-positive aggregates were also seen outside of the SC (**D**, arrows) in a significantly greater number ($P = 0.024$) of cKO pachytene-stage spreads compared to WT (**C**). Normal diplotene phase chromosome spreads with desynapsing chromosomes were observed in both WT (**E**) and cKO (**F**). SYCP1 was absent and SYCP3 was localized to confined foci, consistent with prometaphase, in both WT (**G**) and cKO (**H**) chromosome spread preparations. In addition to typical bright SYCP3 foci, numerous dim foci were observed in the cKO (**H**, crossed arrows). **I**) Bar graph of the number of bright, dim, and total SYCP3 foci in prometaphase spermatocyte spreads with average foci number included from at least 10 spermatocytes for three biological replicates in WT and cKO. **J**) Scatter plots of all the individual spermatocyte SYCP3 foci counts for 52 WT and 52 cKO spermatocyte spreads with mean values indicated with a bar. Asterisk (*) indicates statistically significant difference. Bars in **D** and **H** = 10 µm and are representative of all panels.

In this study, SYCP3 and SYCP1 antibodies were used to track chromosomal dynamics in CDK1-null spermatocytes in prophase I (leptotene, zygotene, pachytene, and diakinesis/prometaphase stages) (Fig. 3). There were no apparent differences in the localization of SYCP3 and SYCP1 in SCs of WT and cKO spermatocytes up to the pachytene stage of meiotic prophase (Fig. 3, A and B). At the pachytene stage when chromosomes are fully synapsed, SYCP3 and SYCP1 colocalized to the SC in all autosomes, and only the unpaired regions of the sex chromosomes lacked SYCP1 (Fig. 3, A and B, arrowhead). Although there were normal complements of synapses, there also was a suggestion of anomalies in CDK1-null pachytene-stage spermatocytes. SYCP3-positive extrasynaptonemal fragments were seen in surface spreads of both WT and cKO pachytene-stage spermatocytes; however, counts of fragments in 30 or more randomly selected spermatocyte spreads from each of five cKO and four WT adult mice found the fragments occurred in 23% of cells in cKO spreads (Fig. 3, C and D, arrows) and less than 7% of cells in WT spreads (Fig. 3C). The fragments often were clustered near pericentromeric heterochromatin and were observed in spermatocytes of both adults and pubertal males in the first wave of spermatogenesis (Supplemental Fig. S3). Whereas the fragments could be generated during the surface spread procedure, the increase in frequency in spreads of cKO spermatocytes suggests a change in SYCP3 localization or stability in these cells. However, the effects of this were not sufficient to prevent CDK1-null spermatocytes from progressing beyond the pachytene stage.

In addition, diplotene-stage spermatocytes with homologous chromosomes undergoing desynapsis and SCs with diminished SYCP1 were seen in surface spreads from both WT (Fig. 3E) and cKO testes (Fig. 3F). These results suggest that CDK1-null spermatocytes are capable of progressing through prophase I of meiosis.

Prometaphase I spermatocytes with compact SYCP3 foci were present, but infrequent, in the spreads in both WT (Fig. 3G) and cKO testes (Fig. 3H). However, the SYCP3 foci that were seen in spreads of cKO testes often appeared abnormal with lesser numbers and intensity of SYCP3 foci. A quantitative analysis of SYCP3 foci in prometaphase spermatocyte spreads revealed a significant decrease in the number of bright SYCP3 foci characteristic of this substage as well as a significant increase in dim foci (Fig. 3I). The dim foci counted were punctate (Fig. 3H, crossed arrows) rather than linear as is often seen late in the diplotene stage during SYCP3 relocalization [37]. The nature of these dim foci was not investigated further but it is likely that they do not all represent relocalized centromeric foci because the total foci count exceeds the expected number of 40 in many spreads. When the total including bright and dim foci are analyzed, there is a significant net decrease in total counts (Fig. 3I). A significant

difference in variability between genotypes was also found for bright, dim, and total foci counts that is appreciable when individual spread counts are graphed (Fig. 3J). These data suggest that the failure to form spermatids is due to defects occurring in prometaphase and metaphase I spermatocytes. Meiotic failure at this stage of spermatocyte development appears to be consistent regardless of the age of the animal. Relocalization of SYCP3 to centromeric foci in prometaphase spermatocytes was also observed in the first wave of spermatogenesis in pubertal animals (not shown) with subsequent lack of spermatids similar to observations in the adult.

Further studies were carried out with antibodies for other markers of progression through prophase I to confirm whether normal prophase progression seen with SYCP3 and SYCP1 extended to other critical prophase events (Supplemental Fig. S4). These other key events of meiotic progression include recombination and repair of double-strand breaks (DSBs) and the subsequent progression to metaphase I [42–44]. Factors involved in this aspect of meiosis include phosphorylated H2AFXγ, ATR, and breast cancer 1 (BRCA1) proteins [45, 46]. These are not only markers of DSBs that occur in leptotene and are repaired by early pachytene stage, but are essential for homologous recombination and formation of chiasmata as well as being necessary for proper chromosomal dynamics and segregation at metaphase. They also become localized to the X-Y body in pachytene-stage spermatocytes [45–47]. In the current study H2AFXγ, ATR, and BRAC1 proteins had the same localization patterns throughout prophase I in WT and cKO spermatocytes (Supplemental Fig. S4, A–J), suggesting DSB repair and the localization of these proteins to the X-Y body do not require CDK1.

Additional markers were examined to determine if a lack of CDK1 disrupts centromere and telomere dynamics in spermatocytes. TERF1 is a component of meiotic telomeres and used to track telomere dynamics through the diplotene stage. Previous studies associated mutations affecting DSB formation and repair and homologous recombination with extended bouquet stage clustering of telomeres [48]. ACA and H3K9me3 label centromeres and heterochromatin, respectively. These markers have been used to monitor centromeric heterochromatin formation, including abnormal centromere clustering in CCNA1-null spermatocytes that arrest at the diplotene stage [13]. However, cKO and WT spermatocytes showed comparable localizations of centromeric heterochromatin and telomeres (Supplemental Fig. S4, K–P).

Also, MLH1 is a marker for the formation of chiasmata during meiosis [49]. The number of chiasmata formed can be determined at the pachytene stage by counting the number of MLH1 foci on homologous chromosomes labeled with SYCP3. The numbers of chiasmata labeled by MLH1 in spermatocytes were similar in WT and cKO spermatocytes (Supplemental Fig. S4, Q-S). These data indicate that CDK1 is not required for DSB formation and resolution, X-Y body formation, centromere and telomere dynamics, or chiasmata formation during the pachytene and diplotene stages of male meiotic prophase I.

The diminished SYCP3 foci in CDK1-null prometaphase I and metaphase I spermatocytes suggested that meiotic progression was disrupted during these phases. This was investigated further by examining H3 core histone phosphorylation at serine 10 (H3pSer10, Fig. 4, A–D). This phosphorylation is coincident with metaphase progression and is tightly correlated with chromosome condensation in spermatocytes and oocytes [28, 50–52]. In spermatocytes, H3pSer10 first appears after desynapsis in the late diplotene stage as spots at centromeric heterochromatin. The signal then becomes more intense throughout the chromatin during the diakinesis phase and in MI [28]. In some WT and cKO spermatocytes, H3pSer10 localized to heterochromatic spots consistent with the late diplotene stage (Fig. 4D, labeled D), and more intensely throughout the nucleus in many other spermatocytes from WT (Fig. 4, A and B) and cKO mice (Fig. 4D, labeled PM), consistent with prometaphase. However, whereas H3pSer10-positive metaphase spermatocytes were seen in tubule sections from WT mice (Fig. 4B, labeled M), they were not detected in tubule sections from cKO mice. This suggests that cKO spermatocytes progress through the diplotene phase and into prometaphase in vivo, but are not competent to progress through prometaphase into metaphase I.

Chromosomes in CDK1-Null Spermatocytes Are Competent to Condense In Vitro

Fully compacted MI bivalent chromosomes characteristic of prometaphase were observed in surface spreads from WT mice (Fig. 4, E and F), whereas only partially condensed MI chromosomes were found in cKO mice (Fig. 4, G and H). This was consistent with the finding that H3pSer10-positive metaphase spermatocytes were seen in WT testis tubules but not in cKO tubules. Previous studies showed that OA, a PP2A and PP1 phosphatase inhibitor [53], was able to promote metaphase chromosome condensation in vitro. It was suggested that OA promoted metaphase chromosome condensation by causing CDK1 to be constitutively active or by preventing dephosphorylation of CDK substrates [1, 40, 54–56]. To determine if cKO spermatocytes were competent to undergo condensation, spermatocytes were isolated and cultured with or without OA for 5 h. It was found that both WT and cKO spermatocytes were able to form fully condensed MI bivalents (Fig. 4, I and J). Thus, whereas CDK1-null spermatocytes fail to progress through prometaphase to form fully condensed chromosomes and to enter metaphase I in vivo, they are competent to undergo OA-induced chromosome condensation in vitro.

Cell Death Is Delayed in CDK1-Null Spermatocytes

The fate of CDK1-null spermatocytes after they failed to progress beyond prometaphase I or metaphase I remained to be determined. The TUNEL assay first was used to determine if cell death was more frequent in cKO than in HET testes (Fig. 5). TUNEL-positive cells (Fig. 5A, arrows) were seen occasionally in the basal region of the tubules (Fig. 5A, red hashed lines) in WT and HET testes, but many more were seen in cKO testes, predominantly in the luminal side of the seminiferous epithelium (Fig. 5B, arrows). The prometaphase I and metaphase I phases occur during the relatively brief spermatogenic cell cycle stage XII (~ 21 h) and thus are seen in ~ 10% of tubule cross sections in WT testes. However, TUNEL-positive cells were present in the majority of tubule cross sections in cKO testes. This suggested a delay in cell death in cKO spermatocytes after they failed to progress through prometaphase I and metaphase I.

Because cKO testes lack the developing spermatids that are informative for defining the stages of the spermatogenic cycle, a different approach was used to determine when TUNEL-positive spermatocytes were present in cKO testes. This involved using IHC with antibodies to SYCP3 [41, 57] to label SCs and to H2AFXγ [58] to monitor H2AX phosphorylation changes, in combination with TUNEL and DAPI staining (Fig. 6A and Supplemental Fig. S5). In WT testes, H2AFXγ was seen as weak diffuse nuclear labeling in

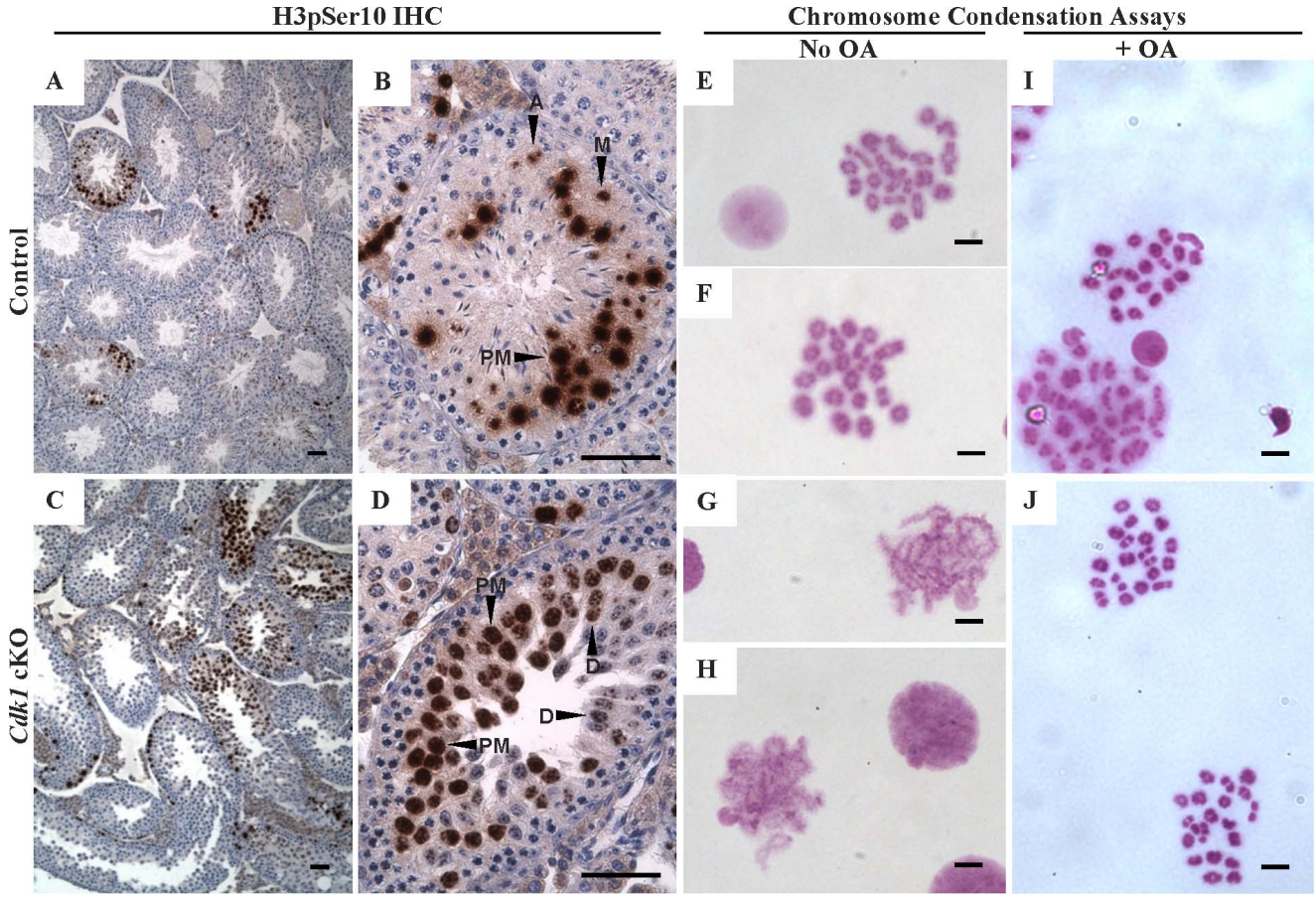

FIG. 4. *Cdk1* cKO spermatocyte chromosomes initiate condensation and fully condense with OA treatment. HET (**A** and **B**) and cKO (**C** and **D**) IHC on testis tissue sections for H3pS10 (brown labeling). Localization to late prophase I/prometaphase spermatocytes is observed in both HET and cKO testis sections (D, diplotene phase; PM, prometaphase) whereas H3pS10 localization in metaphase and later meiotic cells was seen only in the HET (M, metaphase; A, anaphase). **E** and **F**) Air-dried chromosome preparations from WT males showing MI spreads with fully condensed bivalent chromosomes. **G** and **H**) Air-dried chromosome preparations from cKO males contained only partially condensed chromosomes. **I** and **J**) Air-dried chromosome preparations from germ cells pretreated with OA from both WT (**I**) and cKO (**J**) mice both contained MI bivalent chromosomes. Bars in **A**–**D** = 50 μm and in **E**–**J** = 5 μm.

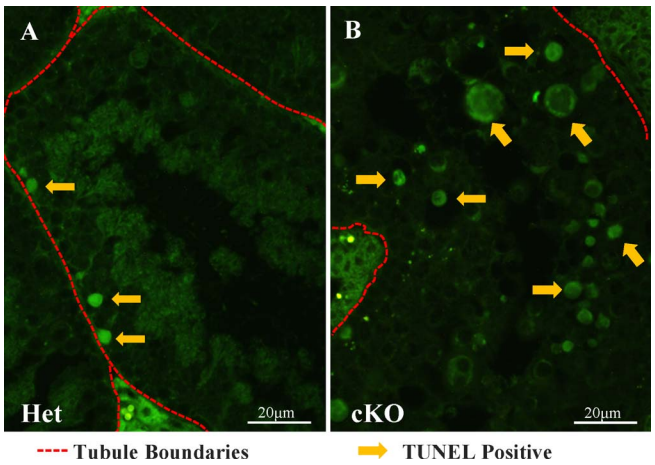

FIG. 5. Increased TUNEL-positive cells in *Cdk1* cKO testes. **A** and **B**) TUNEL staining of testis tubule sections reveals an increased number of apoptotic cells in the luminal half of the seminiferous epithelium in the cKO (**B**) compared to HET mice (**A**). Arrows indicate some TUNEL-positive cells; red hashed lines indicate tubule basal surface/perimeter. Bars = 20 μm.

preleptotene spermatocytes (Fig. 6, stages VII–VIII, arrowheads) and stronger diffuse nuclear labeling in leptotene spermatocytes (Fig. 6A, stages IX–X; arrowheads). The H2AFXγ localized to nuclear foci in zygotene-stage and early pachytene-stage spermatocytes (Fig. 6, stages XI–XII–I, arrowheads) and then to the X-Y body in mid- to late pachytene-stage spermatocytes (Fig. 6, stages II–X, arrows). It was not detectable in diplotene or metaphase phase spermatocytes (stages XI–XII).

These features were used to determine the fraction of tubules and the stages of the spermatogenic cycle containing TUNEL-positive spermatocytes in WT, HET, and cKO testes (Fig. 6, B and C). Whereas 22.3% of tubules in WT and 22.4% of tubules in HET testes contained TUNEL-positive cells, 64.4% of tubules in cKO testes contained TUNEL-positive cells (Fig. 6B). The numbers of TUNEL-positive cKO tubules were significantly higher in all spermatogenic cycle stages except stages XI–I, which trended higher. However, the number of TUNEL-positive cells per TUNEL-positive tubule (Fig. 6C) did exhibit stage-specific differences in total cell death in cKO mice, with the greatest increase in stages VII–VIII. Fewer than four TUNEL-positive cells per TUNEL-positive tubule cross section was seen in WT or HET testes compared to 13 TUNEL-positive cells in cKO testis stages VII–VIII and 6.8 in cKO stages IX–X. This indicates

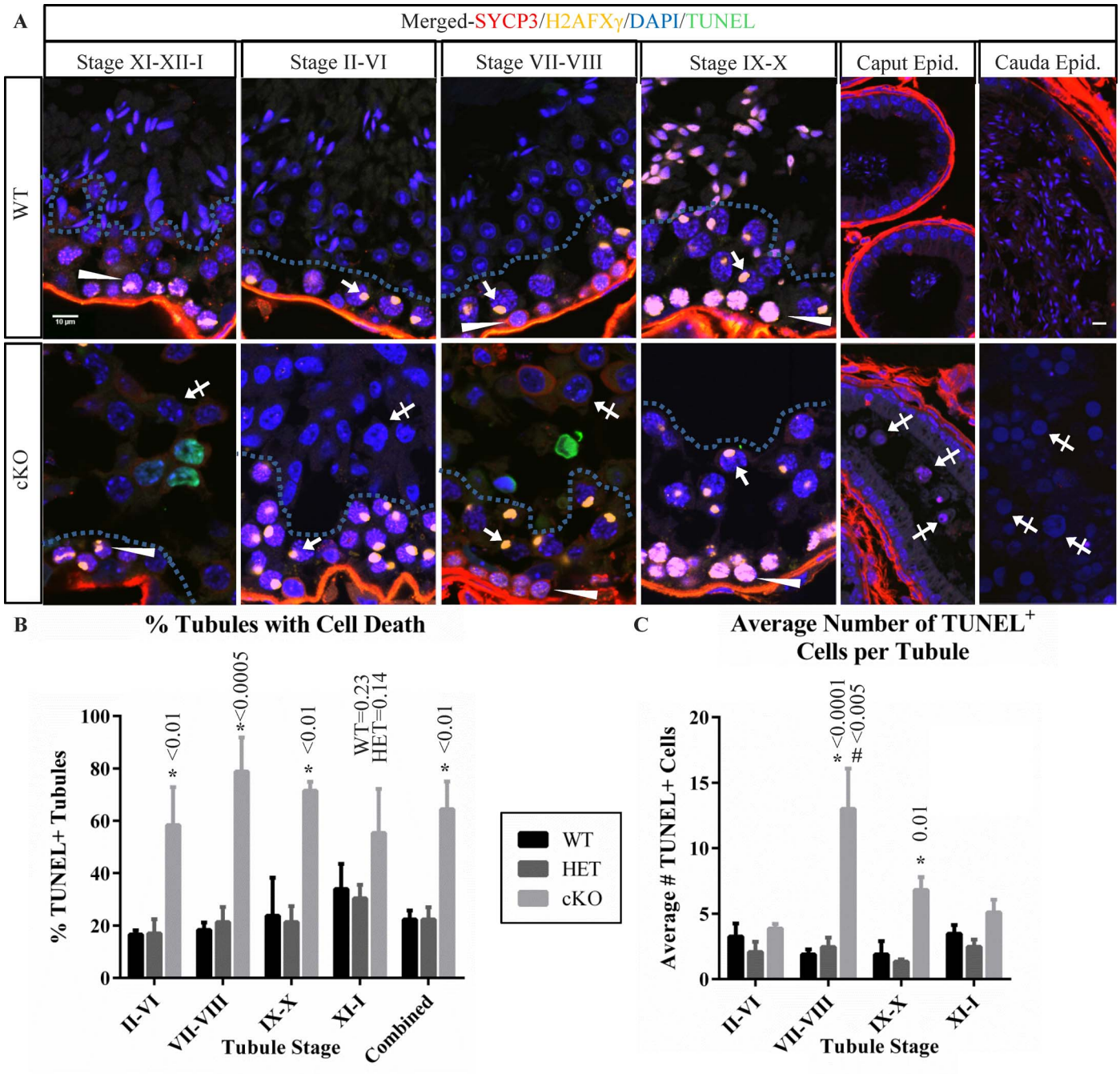

FIG. 6. Germ cell populations in stages of cKO tubules indicate prolonged survival of meiotic arrested germ cells. **A**) Immunofluorescence localization of H2AFXγ (yellow) and SYCP3 (red), along with DAPI staining (blue) was used to group cKO seminiferous tubules into stage-groups and compared to WT. Arrows indicate H2AFXγ in pachytene-stage spermatocytes exhibiting X-Y body localization. Arrowheads indicate weak H2AFXγ chromatin localization in stage VII–VIII preleptotene-stage spermatocytes, strong labeling in stage IX–X leptotene-stage spermatocytes, and patchy labeling in stage XI–XII–I zygotene-stage and zygotene/pachytene-stage transitioning cells, characteristic of H2AFXγ relocalization to the forming XY body. Hashed lines in tubules of testis sections indicate the separation between spermatocytes in the basal portion of the seminiferous epithelium and the spermatids (WT) or abnormal arrested cells (cKO, crossed arrows) in the luminal portion. Cells contained in WT and cKO epididymis are also shown with abnormal cKO cells indicated (crossed arrows). Bars in the upper left and upper right panels are 10 μm and representative for all testis and epididymis panels. **B**) A bar graph summarizing the percent of seminiferous tubules containing TUNEL-positive cells in seminiferous tubules from stage groups II–VI, VII–VIII, IX–X, XI–I, and combined averages in testis sections from WT, HET, and cKO mice. **C**) A bar graph summarizing the number of TUNEL-positive cells per tubule containing such cells. Data for testis sections from each genotype and stage-group are indicated. Error bars represent SEM, asterisk (*) indicates statistically significant difference between genotypes at a given stage, # indicates statistically significant difference between stages for the given genotype. All indicated *P*-value calculations include Tukey multiple testing corrections.

that the increase in TUNEL-positive cells in cKO testes was not coincident with the failure of spermatocytes to progress to metaphase in stage XII, but rather increased significantly in stages VII–VIII of the next seminiferous cycle.

These results indicate that cKO spermatocytes persist in the epithelium after they fail to progress through metaphase in stage XII. In addition to the delay in appearance of TUNEL-positive cells after stage XII, instead of spermatids, cKO germ

cells were seen with large nuclei, irregular nuclear membrane shape, and distinct DAPI-staining heterochromatic DNA foci (Fig. 6A, crossed arrows in cKO panels) in the luminal region of the tubules (Fig. 6A, region of tubule above hashed line). In addition, the nucleoli in these cells contain dense reticulated structures visible in TEM images (Supplemental Fig. 6, A and B, arrows). By identifying the stages of the seminiferous epithelium in cKO testes using SYCP3 and H2AFXγ localization, these cells first become apparent in stage XI–XII–I tubules and remain present until stages VII–VIII, but are infrequent in stages IX–X. The progression of spermatogenesis from stage I to stage VIII takes $\sim$ 5.7 days [59], suggesting that CDK1-null spermatocytes that fail to complete meiosis are retained in the seminiferous epithelium for 5–6 days. The epididymis in cKO mice also contains TUNEL-negative round cells within the ductal lumen (Fig. 6A, cKO caput and cauda epididymis, crossed arrows), suggesting that spermatogenic cells that fail to complete prophase are released into the epididymis without undergoing cell death.

DISCUSSION

Requirement of CDK1 for Completion of MI Is Conserved in Spermatocytes and Oocytes

This study shows for the first time direct evidence that CDK1 is required for completion of meiotic metaphase I progression in male germ cells. Prophase I progresses normally through completion of the diplotene phase in cKO spermatocytes, including chiasmata formation, desynapsis, and initiation of chromosome condensation. The cKO spermatocytes subsequently fail to complete metaphase I, with CDK1 deletion resulting in arrest after the diplotene phase of prophase I and before metaphase I completion. This is consistent with the stage of normal dictyate oocyte arrest in the postnatal ovary at the germinal vesicle stage lasting until after puberty when resumption of meiosis is triggered by extrinsic signals. CDK1 deletion in oocytes leads to an indefinite arrest at this germinal vesicle stage, without meiotic resumption [1]. Thus, CDK1-null spermatocytes and oocytes progress normally through meiotic prophase but are unable to complete metaphase and are instead maintained in an arrested state.

Furthermore, both CDK1-null spermatocytes and oocytes exhibit meiotic progression in the presence of OA. CDK1-null oocytes treated with OA progress through MI including nuclear envelope (germinal vesicle) breakdown following treatment [1]. In the current study, cKO spermatocytes treated with OA are competent to form fully compacted bivalent chromosomes, another hallmark of meiotic metaphase progression. OA is a PP2A and PP1 phosphatase inhibitor, and OA induction of chromosome compaction in WT oocytes and spermatocytes was presumed previously to be via preventing removal of phosphate from CDK1 substrates [1, 40, 54–56]. Indeed, in mitosis, condensins are phosphorylated by CDK1 to initiate chromosome condensation [60]. Additionally, roscovitine inhibition of CDKs in germ cell-Sertoli cell cocultures inhibited postmeiotic germ cell development [61], and the CDK inhibitors staurosporine and butyrolactone I prevented bivalent formation in OA-treated spermatocytes [54]. EIF4G3-null spermatocytes that fail to activate CDK1 also did not condense chromosomes in response to OA treatment [17]. We postulate that because cKO spermatocytes do not have CDK1 phosphorylated proteins to protect, chromosome condensation in CDK1-null spermatocytes following OA treatment was not through prevention of the dephosphorylation of CDK1 substrates. Because OA inhibits the PP2A and PP1 phosphatases, it is possible that the inhibition of phosphatase, directly or indirectly, is a significant functional role for CDK1 in spermatocyte chromatin condensation. In this case, it is the subsequent block of dephosphorylation of PP2A or PP1 substrates that allows completion of chromosome condensation. This model suggests that a lack of CDK1 prevents inhibition of PP1 and/or PP2A phosphatase activity in spermatocytes. Thus, the lack of inhibition of these phosphatases can be overcome by treating with OA to allow chromatin condensation. A similar role for CDK1 in negative regulation of PP1 for germinal vesicle breakdown in the oocyte has been suggested [1]. Thus, a major role for CDK1 in both oocyte and spermatocyte metaphase I progression is possibly via negative regulation of phosphatases. In mitotic cells and in female meiotic cells, CDK1 can inhibit PP2A indirectly through microtubule-associated serine/threonine kinase-like kinase (MASTL, also known as Greatwall) [62, 63] and depletion of MASTL leads to defective chromosome condensation and prometaphase arrest [64, 65]. The present data leave open the possible involvement of MASTL in spermatocyte chromosome condensation but suggest a mechanism other than downstream dephosphorylation of CDK1 substrates occurring in CDK1-null spermatocytes.

CDK1-Null Spermatocytes Bypass Meiotic Checkpoints and Exhibit Features of Senescence

Late prophase CDK1-null spermatocytes enter a prolonged period of arrest, both failing to progress through metaphase I and avoiding checkpoint-associated apoptosis. Normal meiotic arrest checkpoints in spermatocytes include midpachytene-stage arrest, which leads to apoptosis in response to DNA repair defects and asynapsis [66, 67], and metaphase I arrest at a spindle assembly checkpoint [36, 68, 69], resulting in apoptosis or metaphase-anaphase transition mediated by the anaphase-promoting complex. The survival of many CDK1-null spermatocytes beyond stage XII in the seminiferous epithelium suggests dissociation of meiotic failure from checkpoint-mediated cell death in these cells. This is consistent with an upstream role of CDK1 in both metaphase progression and checkpoint function. However, in the absence of CDK1, male- and female-arrested meiocytes exhibit differences in long-term stability. Arrested CDK1-null oocytes do not appear to degenerate, instead maintaining normal morphology [1]. However, we observed many cellular abnormalities in CDK1-null germ cells arresting in the seminiferous epithelium beyond failed metaphase progression at stage XII. In addition to the cells inability to divide, arrested cKO spermatocytes have enlarged nuclei, irregular nuclear/nuclear membrane shape, heterochromatic foci, and distinct nucleoli with temporally diffuse increases in cell death after arrest. These are also characteristics of senescent cells [70, 71]. Negative regulation of CDKs has been implicated in cellular senescence including senescence at G2 of the cell cycle (for a review, see [72]) and our observations seem to support a role for CDK1 suppression in particular cellular pathologies associated with senescence in G2. Interestingly, CDK1-null oocytes were not reported to have abnormal cellular morphology and instead were arrested in an apparently functional suspended state that could be rescued by injecting *Cdk1* mRNA [1]. Given that the arrest point for CDK1-null oocytes is also a natural arrest point for germinal vesicle-stage oocytes, it seems likely that unique mechanisms exist in the oocyte, but not the spermatocyte, to prevent senescence-like cellular changes in the absence of CDK1 expression.

Additional Insights into CDK1-Dependent and -Independent Functions

Desynapsis marks the completion of the diplotene stage in meiotic prophase I and occurs when the central element of the SC, including SYCP1, is removed, releasing homologous chromosomes. HSPA2 is a testis-specific chaperone for CDK1 that in part associates with the SC [15, 73]. Previous studies showed a lack of HSPA2 prevented MPF activation and caused defects in desynapsis of homologous chromosomes [14]. This suggested that desynapsis may be controlled by CDK1 in spermatocytes. However, simultaneous treatment of spermatocytes with OA to promote G2/M transition and with general aurora kinase (AURK) or CDK inhibitors revealed that central element disassembly may not depend on AURKs or CDKs [28]. The combined studies left in question whether the in vitro treatments with chemical inhibitors were specific or if HSPA2 has CDK1-independent functions. Our results indicate that desynapsis is not dependent on CDK1 because it occurs normally in CDK1-null mouse spermatocytes. This points to a yet unidentified mechanism for HSPA2 in regulating desynapsis, independent of its role as a chaperone for CDK1 activation.

Dynamic changes of the SC subsequent to desynapsis, including relocalization of SYCP3 to centromeric regions, are required for chromosome condensation, centromere pairing, and sister chromatid cohesion [27, 37]. These events are in turn important for kinetochore attachment, chromosomal orientation, and resolution of chiasmata. Previous studies testing simultaneous treatment of spermatocytes with OA to promote G2/M transition and with inhibitors of AURK or CDK1 suggest that SYCP3 relocalization is mediated by members of one or both of these kinase families because relocalization is blocked by these treatments [28]. The present studies have shown that relocalization of SYCP3 from the lateral elements of the SC to a more restricted region does not depend on CDK1. Interestingly, CCNA1-null spermatocytes arrest after desynapsis and fail to induce H3pSer10, condense MI chromosomes, or activate MPF [11–13]. In light of our finding that CDK1 is not required for relocalization of SYCP3, induction of H3pSer10, or initiation of chromosome condensation, it will be of further interest to determine if CCNA1, possibly with CDK2, regulates these processes in metaphase I in spermatocytes.

The SC is essential for homolog pairing, synapsis, and chiasmata formation. While synapsis and desynapsis appear to occur normally in cKO spermatocytes, the earliest defect detected in CDK1-null spermatocytes was aberrant localization of some SYCP3 in pachytene-stage spermatocyte spreads. SYCP3 normally is restricted specifically to the SC lateral elements in pachytene-stage spermatocytes; however, cKO pachytene-stage spermatocyte spreads included a significant increase in SYCP3 aggregates not associated with the SC. These were seen along with a normal complement of synapsed homologs with colocalized SYCP3 and SYCP1. It has been shown that SYCP3 and SYCP1 can self-assemble into multimers in vivo [74, 75] and form cytoplasmic aggregates in vivo [38, 57]. Although the SYCP3 fragments seen in this study could be formed in vivo or during the spreading preparation process, the significant difference in occurrence between cKO compared to WT or HET suggests that CDK1 may play a role in restricting assembly of SYCP3 to the lateral elements of the spermatocyte SC. This also suggests a CCNB1-independent function for CDK1 in spermatocytes because CCNB1-mediated MPF activity does not occur until after the diplotene stage. Furthermore abnormalities in the relocalization of SYCP3 to centromeric foci in the cKO diakinesis/prometaphase stage also suggest a role for CDK1 upstream of the regulation of SYCP3 localization.

In summary, the results of these studies indicate that CDK1 is required for completion of metaphase I in spermatocytes, including condensation of bivalent chromosomes. OA compaction of cKO spermatocyte chromosomes suggests that negative regulation of phosphatases is a key role of CDK1 in spermatocytes. Whereas CDKs have been shown to have redundant roles in many systems, this study suggests that other CDKs, including CDK2 [5], do not compensate for lack of CDK1 for spermatocyte metaphase progression. Thus, both CDK1 and CDK2 play essential roles in male germ cell meiosis. Although female meiocytes do not require CDK2 and differ from spermatocytes in the roles of alternative cell cycle kinases previously reported, as well as for CDK1 regulation and binding partners, the role of CDK1 is apparently conserved between male and female meiocytes. CDK1-null spermatocytes progress through prophase and arrest prior to completion of metaphase I, exhibiting a prolonged arrest in late prophase. We also show here for the first time that deletion of CDK1 affects SYCP3 localization and late meiosis I spermatocyte nucleolar morphology, but not the ability of bivalent spermatocyte chromosomes to condense in response to OA treatment.

ACKNOWLEDGMENT

We would like to thank Mary Ann Handel, Pat Hunt, and Crystal Lawson for technical guidance; Mary Ann Handel, Greg Buchold, Barbara Nicol, Silvia Hewitt, and members of the Gamete Biology Group for insightful comments; Linwood Koonce for assistance in maintaining animal colonies; Grace Kissling for providing statistical expertise; and the NIEHS Confocal Microscopy Core. ALI, TMC, and EME planned the studies and analyzed the results. ALI generated the targeting vector, WDW performed the ES cell cultures, ALI and WDW screened the ES cell clones, EHG injected the ES cells into blastocysts, and ALI initiated and TMC completed the cKO phenotyping studies. TMC performed ISH, cell death assays, spermatocyte surface spreads, chromosome preparations, and condensation assays, and TMC and EME performed TEM and wrote the manuscript. All the authors reviewed and revised the manuscript.

REFERENCES

1. Adhikari D, Zheng W, Shen Y, Gorre N, Ning Y, Halet G, Kaldis P, Liu K. Cdk1, but not Cdk2, is the sole Cdk that is essential and sufficient to drive resumption of meiosis in mouse oocytes. Hum Mol Genet 2012; 21: 2476–2484.
2. Diril MK, Ratnacaram CK, Padmakumar VC, Du T, Wasser M, Coppola V, Tessarollo L, Kaldis P. Cyclin-dependent kinase 1 (Cdk1) is essential for cell division and suppression of DNA re-replication but not for liver regeneration. Proc Natl Acad Sci U S A 2012; 109:3826–3831.
3. Santamaria D, Barriere C, Cerqueira A, Hunt S, Tardy C, Newton K, Caceres JF, Dubus P, Malumbres M, Barbacid M. Cdk1 is sufficient to drive the mammalian cell cycle. Nature 2007; 448:811–815.
4. Ortega S, Prieto I, Odajima J, Martin A, Dubus P, Sotillo R, Barbero JL, Malumbres M, Barbacid M. Cyclin-dependent kinase 2 is essential for meiosis but not for mitotic cell division in mice. Nat Genet 2003; 35: 25–31.
5. Berthet C, Aleem E, Coppola V, Tessarollo L, Kaldis P. Cdk2 knockout mice are viable. Curr Biol 2003; 13:1775–1785.
6. Kishimoto T. Cell-cycle control during meiotic maturation. Curr Opin Cell Biol 2003; 15:654–663.
7. Lincoln AJ, Wickramasinghe D, Stein P, Schultz RM, Palko ME, De Miguel MP, Tessarollo L, Donovan PJ. Cdc25b phosphatase is required for resumption of meiosis during oocyte maturation. Nat Genet 2002; 30: 446–449.
8. Chua SS, Ma Z, Ngan E, Tsai SY. Cdc25B as a steroid receptor coactivator. Vitam Horm 2004; 68:231–256.
9. Touati SA, Cladiere D, Lister LM, Leontiou I, Chambon JP, Rattani A, Bottger F, Stemmann O, Nasmyth K, Herbert M, Wassmann K. Cyclin A2 is required for sister chromatid segregation, but not separase control, in mouse oocyte meiosis. Cell Rep 2012; 2:1077–1087.
10. Ravnik SE, Wolgemuth DJ. Regulation of meiosis during mammalian

spermatogenesis: the A-type cyclins and their associated cyclin-dependent kinases are differentially expressed in the germ-cell lineage. Dev Biol 1999; 207:408–418.
11. Liu D, Liao C, Wolgemuth DJ. A role for cyclin A1 in the activation of MPF and G2-M transition during meiosis of male germ cells in mice. Dev Biol 2000; 224:388–400.
12. Liu D, Matzuk MM, Sung WK, Guo Q, Wang P, Wolgemuth DJ. Cyclin A1 is required for meiosis in the male mouse. Nat Genet 1998; 20: 377–380.
13. Nickerson HD, Joshi A, Wolgemuth DJ. Cyclin A1-deficient mice lack histone H3 serine 10 phosphorylation and exhibit altered aurora B dynamics in late prophase of male meiosis. Dev Biol 2007; 306:725–735.
14. Dix DJ, Allen JW, Collins BW, Poorman-Allen P, Mori C, Blizard DR, Brown PR, Goulding EH, Strong BD, Eddy EM. HSP70-2 is required for desynapsis of synaptonemal complexes during meiotic prophase in juvenile and adult mouse spermatocytes. Development 1997; 124: 4595–4603.
15. Zhu D, Dix DJ, Eddy EM. HSP70-2 is required for CDC2 kinase activity in meiosis I of mouse spermatocytes. Development 1997; 124:3007–3014.
16. Mori C, Allen JW, Dix DJ, Nakamura N, Fujioka M, Toshimori K, Eddy EM. Completion of meiosis is not always required for acrosome formation in HSP70-2 null mice. Biol Reprod 1999; 61:813–822.
17. Sun F, Palmer K, Handel MA. Mutation of Eif4g3, encoding a eukaryotic translation initiation factor, causes male infertility and meiotic arrest of mouse spermatocytes. Development 2010; 137:1699–1707.
18. Solc P, Schultz RM, Motlik J. Prophase I arrest and progression to metaphase I in mouse oocytes: comparison of resumption of meiosis and recovery from G2-arrest in somatic cells. Mol Hum Reprod 2010; 16: 654–664.
19. Inselman AL, Nakamura N, Brown PR, Willis WD, Goulding EH, Eddy EM. Heat shock protein 2 promoter drives Cre expression in spermatocytes of transgenic mice. Genesis 2010; 48:114–120.
20. Leuchtenberger C, Schrader F. The chemical nature of the acrosome in the male germ cells. Proc Natl Acad Sci U S A 1950; 36:677–683.
21. Maekawa M, O'Brien DA, Allen RL, Eddy EM. Heat-shock cognate protein (hsc71) and related proteins in mouse spermatogenic cells. Biol Reprod 1989; 40:843–852.
22. Bunch DO, Welch JE, Magyar PL, Eddy EM, O'Brien DA. Glyceraldehyde 3-phosphate dehydrogenase-S protein distribution during mouse spermatogenesis. Biol Reprod 1998; 58:834–841.
23. Meehan T, Schlatt S, O'Bryan MK, de Kretser DM, Loveland KL. Regulation of germ cell and Sertoli cell development by activin, follistatin, and FSH. Dev Biol 2000; 220:225–237.
24. Murdoch B, Owen N, Shirley S, Crumb S, Broman KW, Hassold T. Multiple loci contribute to genome-wide recombination levels in male mice. Mamm Genome 2010; 21:550–555.
25. Peters AH, Plug AW, van Vugt MJ, de Boer P. A drying-down technique for the spreading of mammalian meiocytes from the male and female germline. Chromosome Res 1997; 5:66–68.
26. Dresser ME, Moses MJ. Synaptonemal complex karyotyping in spermatocytes of the Chinese hamster (Cricetulus griseus). IV. Light and electron microscopy of synapsis and nucleolar development by silver staining. Chromosoma 1980; 76:1–22.
27. Qiao H, Chen JK, Reynolds A, Hoog C, Paddy M, Hunter N. Interplay between synaptonemal complex, homologous recombination, and centromeres during mammalian meiosis. PLoS Genet 2012; 8:e1002790.
28. Sun F, Handel MA. Regulation of the meiotic prophase I to metaphase I transition in mouse spermatocytes. Chromosoma 2008; 117:471–485.
29. O'Brien DA. Isolation, separation, and short term culture of spermatogenic cells. In: Chapin RE, Heindel JJ (eds.), Methods in Toxicology, vol. 3A: Male Reproductive Toxicology. San Diego, CA: Academic Press Inc.; 1993:246–264.
30. Evans EP, Breckon G, Ford CE. An air-drying method for meiotic preparations from mammalian testes. Cytogenetics 1964; 3:289–294.
31. Wiltshire T, Park C, Caldwell KA, Handel MA. Induced premature G2/M-phase transition in pachytene spermatocytes includes events unique to meiosis. Dev Biol 1995; 169:557–567.
32. Miki K, Willis WD, Brown PR, Goulding EH, Fulcher KD, Eddy EM. Targeted disruption of the Akap4 gene causes defects in sperm flagellum and motility. Dev Biol 2002; 248:331–342.
33. Fawcett DW, Ito S, Slautterback D. The occurrence of intercellular bridges in groups of cells exhibiting synchronous differentiation. J Biophys Biochem Cytol 1959; 5:453–460.
34. Holstein AF, Eckmann C. Multinucleated spermatocytes and spermatids in human seminiferous tubules. Andrologia 1986; 18:5–16.
35. Bolcun-Filas E, Schimenti JC. Genetics of meiosis and recombination in mice. Int Rev Cell Mol Biol 2012; 298:179–227.
36. Handel MA, Schimenti JC. Genetics of mammalian meiosis: regulation, dynamics and impact on fertility. Nat Rev Genet 2010; 11:124–136.
37. Bisig CG, Guiraldelli MF, Kouznetsova A, Scherthan H, Hoog C, Dawson DS, Pezza RJ. Synaptonemal complex components persist at centromeres and are required for homologous centromere pairing in mouse spermatocytes. PLoS Genet 2012; 8:e1002701.
38. de la Fuente R, Parra MT, Viera A, Calvente A, Gomez R, Suja JA, Rufas JS, Page J. Meiotic pairing and segregation of achiasmate sex chromosomes in eutherian mammals: the role of SYCP3 protein. PLoS Genet 2007; 3:e198.
39. Jordan PW, Karppinen J, Handel MA. Polo-like kinase is required for synaptonemal complex disassembly and phosphorylation in mouse spermatocytes. J Cell Sci 2012; 125:5061–5072.
40. Tarsounas M, Pearlman RE, Moens PB. Meiotic activation of rat pachytene spermatocytes with okadaic acid: the behaviour of synaptonemal complex components SYN1/SCP1 and COR1/SCP3. J Cell Sci 1999; 112(Pt 4):423–434.
41. Yuan L, Liu JG, Zhao J, Brundell E, Daneholt B, Hoog C. The murine SCP3 gene is required for synaptonemal complex assembly, chromosome synapsis, and male fertility. Mol Cell 2000; 5:73–83.
42. Dobson MJ, Pearlman RE, Karaiskakis A, Spyropoulos B, Moens PB. Synaptonemal complex proteins: occurrence, epitope mapping and chromosome disjunction. J Cell Sci 1994; 107(Pt 10):2749–2760.
43. Lammers JH, Offenberg HH, van Aalderen M, Vink AC, Dietrich AJ, Heyting C. The gene encoding a major component of the lateral elements of synaptonemal complexes of the rat is related to X-linked lymphocyte-regulated genes. Mol Cell Biol 1994; 14:1137–1146.
44. Meuwissen RL, Offenberg HH, Dietrich AJ, Riesewijk A, van Iersel M, Heyting C. A coiled-coil related protein specific for synapsed regions of meiotic prophase chromosomes. EMBO J 1992; 11:5091–5100.
45. Celeste A, Petersen S, Romanienko PJ, Fernandez-Capetillo O, Chen HT, Sedelnikova OA, Reina-San-Martin B, Coppola V, Meffre E, Difilippantonio MJ, Redon C, Pilch DR, et al. Genomic instability in mice lacking histone H2AX. Science 2002; 296:922–927.
46. Xu X, Aprelikova O, Moens P, Deng CX, Furth PA. Impaired meiotic DNA-damage repair and lack of crossing-over during spermatogenesis in BRCA1 full-length isoform deficient mice. Development 2003; 130: 2001–2012.
47. Yanowitz J. Meiosis: making a break for it. Curr Opin Cell Biol 2010; 22: 744–751.
48. Liebe B, Petukhova G, Barchi M, Bellani M, Braselmann H, Nakano T, Pandita TK, Jasin M, Fornace A, Meistrich ML, Baarends WM, Schimenti J, et al. Mutations that affect meiosis in male mice influence the dynamics of the mid-preleptotene and bouquet stages. Exp Cell Res 2006; 312: 3768–3781.
49. Baker SM, Plug AW, Prolla TA, Bronner CE, Harris AC, Yao X, Christie DM, Monell C, Arnheim N, Bradley A, Ashley T, Liskay RM. Involvement of mouse Mlh1 in DNA mismatch repair and meiotic crossing over. Nat Genet 1996; 13:336–342.
50. Bui HT, Yamaoka E, Miyano T. Involvement of histone H3 (Ser10) phosphorylation in chromosome condensation without Cdc2 kinase and mitogen-activated protein kinase activation in pig oocytes. Biol Reprod 2004; 70:1843–1851.
51. Swain JE, Ding J, Brautigan DL, Villa-Moruzzi E, Smith GD. Proper chromatin condensation and maintenance of histone H3 phosphorylation during mouse oocyte meiosis requires protein phosphatase activity. Biol Reprod 2007; 76:628–638.
52. Swain JE, Ding J, Wu J, Smith GD. Regulation of spindle and chromatin dynamics during early and late stages of oocyte maturation by aurora kinases. Mol Hum Reprod 2008; 14:291–299.
53. Cohen P, Holmes CF, Tsukitani Y. Okadaic acid: a new probe for the study of cellular regulation. Trends Biochem Sci 1990; 15:98–102.
54. Cobb J, Cargile B, Handel MA. Acquisition of competence to condense metaphase I chromosomes during spermatogenesis. Dev Biol 1999; 205: 49–64.
55. Hunt T. On the regulation of protein phosphatase 2A and its role in controlling entry into and exit from mitosis. Adv Biol Regul 2013; 53: 173–178.
56. Inselman A, Handel MA. Mitogen-activated protein kinase dynamics during the meiotic G2/MI transition of mouse spermatocytes. Biol Reprod 2004; 71:570–578.
57. Parra MT, Viera A, Gomez R, Page J, Benavente R, Santos JL, Rufas JS, Suja JA. Involvement of the cohesin Rad21 and SCP3 in monopolar attachment of sister kinetochores during mouse meiosis I. J Cell Sci 2004; 117:1221–1234.
58. Blanco-Rodriguez J. GammaH2AX marks the main events of the spermatogenic process. Microsc Res Tech 2009; 72:823–832.

59. Oakberg EF. Duration of spermatogenesis in the mouse and timing of stages of the cycle of the seminiferous epithelium. Am J Anat 1956; 99: 507–516.
60. Abe S, Nagasaka K, Hirayama Y, Kozuka-Hata H, Oyama M, Aoyagi Y, Obuse C, Hirota T. The initial phase of chromosome condensation requires Cdk1-mediated phosphorylation of the CAP-D3 subunit of condensin II. Genes Dev 2011; 25:863–874.
61. Godet M, Damestoy A, Mouradian S, Rudkin BB, Durand P. Key role for cyclin-dependent kinases in the first and second meiotic divisions of rat spermatocytes. Biol Reprod 2004; 70:1147–1152.
62. Blake-Hodek KA, Williams BC, Zhao Y, Castilho PV, Chen W, Mao Y, Yamamoto TM, Goldberg ML. Determinants for activation of the atypical AGC kinase Greatwall during M phase entry. Mol Cell Biol 2012; 32: 1337–1353.
63. Vigneron S, Brioudes E, Burgess A, Labbe JC, Lorca T, Castro A. Greatwall maintains mitosis through regulation of PP2A. EMBO J 2009; 28:2786–2793.
64. Alvarez-Fernandez M, Sanchez-Martinez R, Sanz-Castillo B, Gan PP, Sanz-Flores M, Trakala M, Ruiz-Torres M, Lorca T, Castro A, Malumbres M. Greatwall is essential to prevent mitotic collapse after nuclear envelope breakdown in mammals. Proc Natl Acad Sci U S A 2013; 110: 17374–17379.
65. Hara M, Abe Y, Tanaka T, Yamamoto T, Okumura E, Kishimoto T. Greatwall kinase and cyclin B-Cdk1 are both critical constituents of M-phase-promoting factor. Nat Commun 2012; 3:1059.
66. Roeder GS, Bailis JM. The pachytene checkpoint. Trends Genet 2000; 16: 395–403.
67. Barchi M, Mahadevaiah S, Di Giacomo M, Baudat F, de Rooij DG, Burgoyne PS, Jasin M, Keeney S. Surveillance of different recombination defects in mouse spermatocytes yields distinct responses despite elimination at an identical developmental stage. Mol Cell Biol 2005; 25: 7203–7215.
68. Oka A, Mita A, Takada Y, Koseki H, Shiroishi T. Reproductive isolation in hybrid mice due to spermatogenesis defects at three meiotic stages. Genetics 2010; 186:339–351.
69. Eaker S, Pyle A, Cobb J, Handel MA. Evidence for meiotic spindle checkpoint from analysis of spermatocytes from Robertsonian-chromosome heterozygous mice. J Cell Sci 2001; 114:2953–2965.
70. Mehta IS, Figgitt M, Clements CS, Kill IR, Bridger JM. Alterations to nuclear architecture and genome behavior in senescent cells. Ann N Y Acad Sci 2007; 1100:250–263.
71. Narita M, Nunez S, Heard E, Narita M, Lin AW, Hearn SA, Spector DL, Hannon GJ, Lowe SW. Rb-mediated heterochromatin formation and silencing of E2F target genes during cellular senescence. Cell 2003; 113: 703–716.
72. Gire V, Dulic V. Senescence from G2 arrest, revisited. Cell Cycle 2015; 14:297–304.
73. Allen JW, Dix DJ, Collins BW, Merrick BA, He C, Selkirk JK, Poorman-Allen P, Dresser ME, Eddy EM. HSP70-2 is part of the synaptonemal complex in mouse and hamster spermatocytes. Chromosoma 1996; 104: 414–421.
74. Ollinger R, Alsheimer M, Benavente R. Mammalian protein SCP1 forms synaptonemal complex-like structures in the absence of meiotic chromosomes. Mol Biol Cell 2005; 16:212–217.
75. Yuan L, Pelttari J, Brundell E, Bjorkroth B, Zhao J, Liu JG, Brismar H, Daneholt B, Hoog C. The synaptonemal complex protein SCP3 can form multistranded, cross-striated fibers in vivo. J Cell Biol 1998; 142:331–339.
76. Dix DJ, Allen JW, Collins BW, Mori C, Nakamura N, Poorman-Allen P, Goulding EH, Eddy EM. Targeted gene disruption of Hsp70-2 results in failed meiosis, germ cell apoptosis, and male infertility. Proc Natl Acad Sci U S A 1996; 93:3264–3268.
77. National Institutes of Health. An efficient and cost-effective assay for genotyping mice using melt curve analysis. http://www.ott.nih.gov/technology/e-064-2012. Accessed August 26, 2015.